© &d

Eri1 degrades the stem-loop of oligouridylated histone mRNAs to induce replication-dependent decay

Kai P Hoefig¹, Nicola Rath^{1,4,5}, Gitta A Heinz^{1,5}, Christine Wolf¹, Jasmin Dameris¹, Aloys Schepers², Elisabeth Kremmer¹, K Mark Ansel³ & Vigo Heissmeyer¹

The exoRNase Eri1 inhibits RNA interference and trims the 5.8S rRNA 3' end. It also binds to the stem-loop of histone mRNAs, but the functional importance of this interaction remains elusive. Histone mRNAs are normally degraded at the end of S phase or after pharmacological inhibition of replication. Both processes are impaired in Eri1-deficient mouse cells, which instead accumulate oligouridylated histone mRNAs. Eri1 trims the mature histone mRNAs by two unpaired nucleotides at the 3' end but stalls close to the double-stranded stem. Upon oligouridylation of the histone mRNA, the Lsm1–7 heteroheptamer recognizes the oligo(U) tail and interacts with Eri1, whose catalytic activity is then able to degrade the stem-loop in a stepwise manner. These data demonstrate how degradation of histone mRNAs is initiated when 3' oligouridylation creates a *cis* element that enables Eri1 to process the double-stranded stem-loop structure.

Exoribonuclease 1 (Eri1) is a 3' exonuclease that is conserved in eukaryotes from the fission yeast *Schizosaccharomyces pombe* to humans. The *eri1* gene was identified in a screen for inhibitors of the exogenous short interfering RNA (siRNA) pathway in *Caenorhabditis elegans*¹. In *S. pombe*, Eri1 limits the expression of endogenous nuclear siRNAs and their function in heterochromatin formation^{2,3}. Recently, Eri1 was also shown to limit the expression of mature microRNAs (miRNAs) in mouse T and NK cells, without exhibiting specificity for certain miRNA sequences⁴. In addition to regulating exogenous and endogenous RNA-interference (RNAi) function, Eri1 was also found to be critical for 3'-end trimming of the 5.8S rRNA, a function that is conserved in eukaryotes from fission yeast to mammals^{5,6}. *In vitro*, Eri1 degrades single-stranded RNA and 3' overhangs but is strongly inhibited by double-stranded RNA structures^{1,6–8}.

Earlier studies showed that stem-loop-binding protein (SLBP) and human ERI1 (previously also termed 3'hExo or THEX1) bind to replication-dependent (canonical) histone mRNAs^{7,9-11}. These mRNAs are not stabilized through polyadenylation but through a highly conserved stem-loop at their 3' end, which can simultaneously be bound by SLBP and Eri1 proteins *in vitro*^{7,12}. Replication-dependent histone mRNAs of the five classes (1, 2a, 2b, 3 and 4) are initially transcribed as longer precursors from three genomic clusters (Hist1, Hist2 and Hist3) that encode 65 genes in mice¹³. The precursor transcripts are cleaved to form a 3' end that terminates five nucleotides downstream of the stem-loop. Histone expression is tightly coupled to DNA replication to accommodate the newly synthesized DNA in nucleosomes. Histone mRNA levels rapidly increase as the cells enter S phase, to meet the nucleosome demand, and sharply decrease when DNA replication

ceases. The balance of DNA and histone synthesis is important because artificially increased levels of histones can cause chromosome loss and genome instability¹⁴. At the end of S phase, the stem-loop serves as a *cis* element that is required and sufficient to mediate histone mRNA degradation^{15,16}. In comparison, degradation of polyadenylated mRNAs is initiated by deadenylation¹⁷. Typically, the oligo(A) tail is recognized by the Lsm1–7 complex, which promotes mRNA decapping¹⁸ and rapid 5′-to-3′ degradation, but 3′-to-5′ degradation by the exosome may contribute to mRNA decay as well¹⁹.

It was recently found that histone mRNA oligouridylation at the 3' end preceded degradation. It correlated with the appearance of degradation intermediates that were shortened from the 3' end as well as the 5' end²⁰. Histone mRNA degradation depended on Lsm1 and Upf1 (refs. 20,21) in addition to cellular terminal uridyltransferases (TUTases)^{20,22}. The specific molecular role of the RNA helicase Upf1 in the degradation process remains unclear. Lsm1 is part of the heteroheptameric Lsm1–7 ring, which preferentially binds oligo(U) tails²³. It was therefore proposed that Lsm1–7 initiates decapping of oligouridylated histone mRNAs, similar to its function in the degradation pathway of oligoadenylated mRNAs. By analyzing cells from the Eri1-deficient mouse, we investigated the role of Eri1 in histone mRNA regulation.

RESULTS

Eri1 is required for replication-dependent histone mRNA decay

To investigate functional consequences that may result from the previously reported interaction of the Eri1 protein with the histone mRNA stem-loop^{7,8,12}, we analyzed Eri1-deficient and wild-type mouse

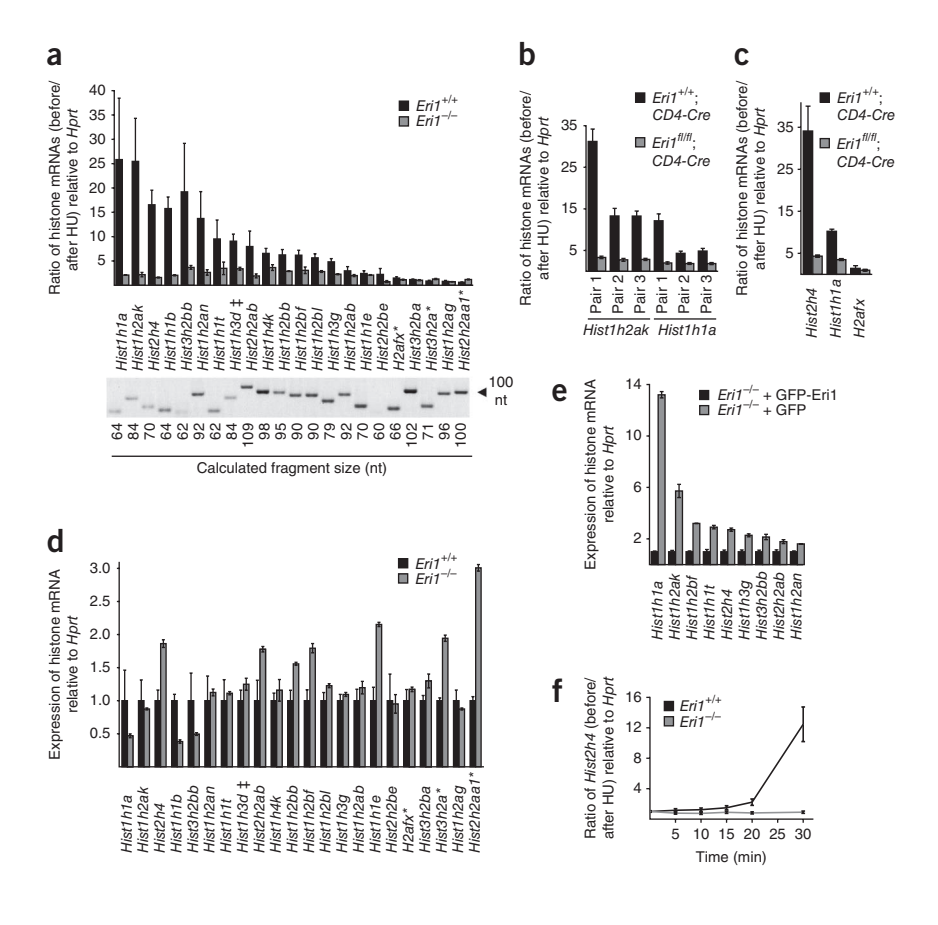
¹Institute of Molecular Immunology, Helmholtz Zentrum München, München, Germany. ²Research Unit Gene Vectors, Helmholtz Zentrum München, München, Germany. ³Department of Microbiology and Immunology, University of California San Francisco, San Francisco, California, USA. ⁴Present address: Beatson Institute for Cancer Research, Glasgow, UK. ⁵These authors contributed equally to this work. Correspondence should be addressed to V.H. (vigo.heissmeyer@helmholtz-muenchen.de).

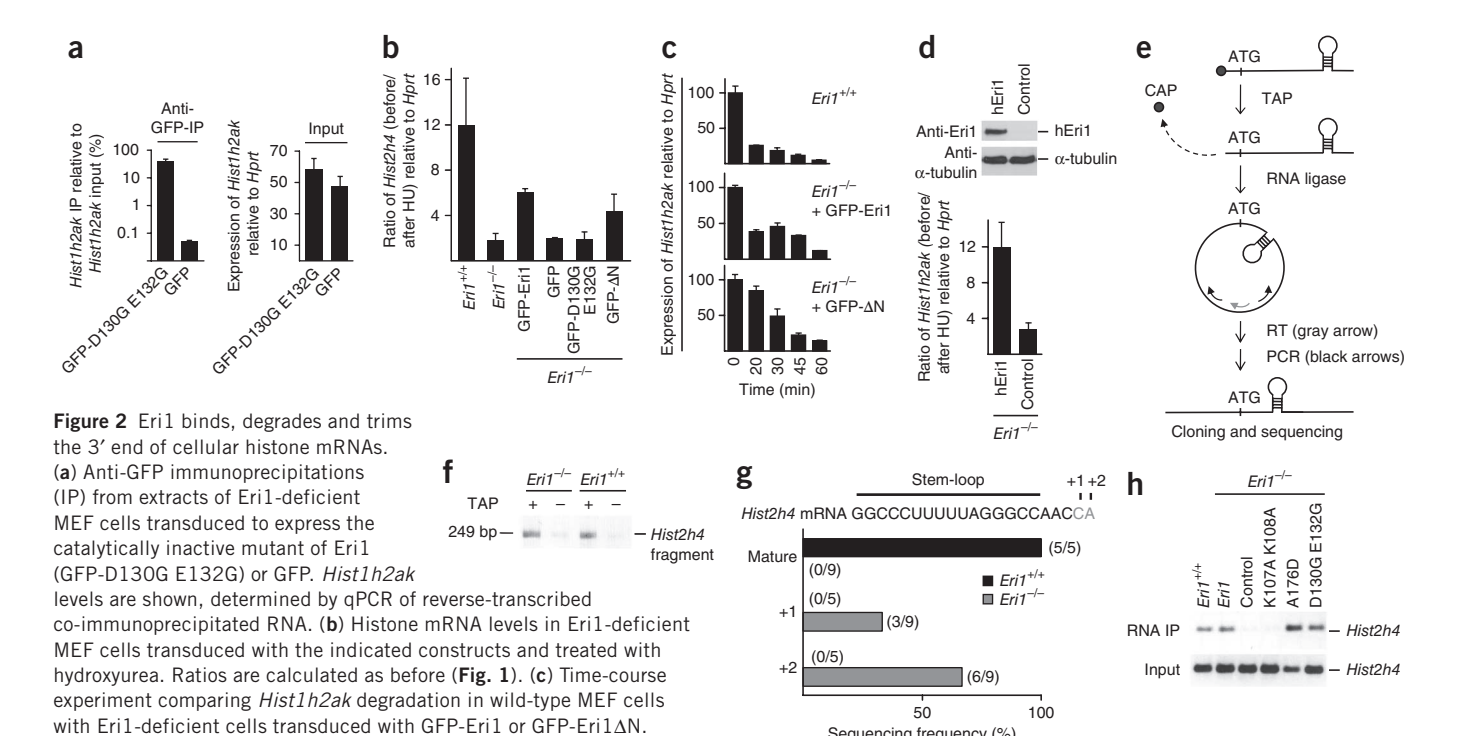
Received 2 March; accepted 16 October; published online 2 December 2012; doi:10.1038/nsmb.2450

embryonic fibroblast (MEF) cells. In these cell lines, we determined the extent to which histone mRNA degradation was induced by the DNA-replication inhibitor hydroxyurea. This pharmacological agent triggers molecular events that affect histone mRNAs in untreated cells at the end of S phase. A panel of 22 histone genes was selected for probe-based quantitative PCR (qPCR) analysis. In wild-type MEF cells, the ratio of histone mRNA expression levels before and 45 min after hydroxyurea treatment showed strongly induced degradation at varying degrees for 17 out of 19 replication-dependent histone mRNAs (Fig. 1a). Hydroxyurea-induced degradation was greatly attenuated in Eri1-deficient MEF cells (Fig. 1a). Analysis of the mRNA levels of the longer isoform of *H2afx* showed no effect in both cell lines (**Fig. 1a**). This is consistent with previous findings indicating that this replication-independent histone mRNA is hardly affected by hydroxyurea treatment on the transcriptional and post-transcriptional level^{24,25}. Loss of Eri1 inhibited the induced downregulation of histone mRNAs of all five classes (H1, H2a, H2b, H3 and H4) and from each of the three gene clusters (Hist1, Hist2 and Hist3). Considering the high degree of sequence similarity among histone genes, we confirmed the specificity of PCR amplification. We cloned and sequence verified representative Hist2h4 and Hist1h2ak amplicons (data not shown) and matched the actual with the calculated amplicon sizes for all 22 qPCR assays (Fig. 1a and Supplementary Table 1). We observed a similar defect in Eri1-deficient primary activated CD4 T cells, when comparing sex- and age-matched animal pairs of both genotypes. As in MEF cells, loss of Eri1 interfered with hydroxyurea-induced histone mRNA degradation, as determined for the replication-dependent genes Hist1h2ak, Hist1h1a (Fig. 1b,c) and Hist2h4 (Fig. 1c), without affecting the expression of the replication-independent *H2afx* histone mRNA (Fig. 1c).

We also compared histone mRNA abundance in unstimulated asynchronously growing MEF cells. The mRNAs of only a few of the analyzed genes were less abundant in Eri1-deficient MEF cells (Fig. 1d, Hist1h1a, Hist1h1b and Hist3h2bb), whereas several of the remaining histone mRNA transcripts had strongly (Fig. 1d, Hist2h4, Hist2h2ab, Hist1h2bb, Hist1h2bf and Hist1h1e) or slightly increased expression as compared to wild-type cells. This panel revealed only a trend toward higher histone mRNA expression in Eri1-deficient cells. We then attempted to avoid differences resulting from cell preparation of different mouse embryos, immortalization and selection, which may manifest individual cell-line compensation for the loss of Eril. Reintroduction of GFP-Eri1 into Eri1-deficient cells decreased the abundance of all replication-dependent histone mRNAs tested, as compared to cells that were transduced to express GFP only (Fig. 1e). Characterizing these retrovirally transduced cells further in immunoblots, we found that exogenous expression of Eri1 exceeded the endogenous levels in wild-type cells by far (Supplementary Fig. 1a). Accordingly, overexpression as well as reconstitution of Eri1 function in Eri1-deficient cells may be reflected in the histone mRNA expression. This, however, did not alter the cell size (Supplementary Fig. 1b) or the cell cycle when compared to co-cultured GFP-negative cells (Supplementary Fig. 1c,d). The observed changes in histone mRNA content after Eri1 overexpression (Fig. 1e) were therefore not secondary to differences in cell-cycle progression. In a time-course experiment, hydroxyurea-induced Hist2h4 mRNA degradation in wild-type MEF cells was markedly increased after 20-30 min of treatment, whereas this mRNA remained unaffected in Eri1-deficient cells (Fig. 1f). These data show that the major cellular pathway of hydroxyurea-induced degradation of histone mRNAs relies on the presence of Eril.

Figure 1 Eri1 is required for the degradation of replication-dependent histone mRNAs. (a) Histone mRNA levels of Eri1-deficient and wild-type MEF cells, quantified before and after hydroxyurea (HU) treatment, showing significantly less degradation of replication-dependent histone mRNAs (n = 19) in Eri1-deficient cells (P = 0.0006) with the paired t-test. Ratios are shown between Hprtnormalized expression at 0 min and 45 min. The lower panel shows qPCR-amplified fragments on a 4% agarose gel. nt, nucleotides. (b,c) The same experiments as in a, but using 44-h-activated Eri1-deficient (Eri1fl/fl; CD4-Cre) and wild-type CD4 T cells (Eri1+/+; CD4-Cre) from four different pairs of littermate mice. The paired t-test was applied over all six comparisons in **b** (P = 0.035). (d,e) Histone mRNA measured by qPCR and compared in Eri1-deficient and wild-type MEF cells (d) or Eri1-deficient MEF cells transduced with GFP-Eri1 or GFP (e). Histone mRNA levels were set to 1 in wild-type and GFP-Eri1 reconstituted cells, respectively. (f) Histone mRNA degradation in Eri1-deficient and wild-type MEF cells in response to hydroxyurea treatment at the indicated time points. Asterisk indicates primers that recognize only the polyadenylated transcripts from the genes; ++ indicates primers that also detect *Hist1h3e*, Hist1h3g, Hist1h3h and Hist1h3i, owing to sequence identity in primer and probe annealing regions. a and d-f are representative of at least two independent experiments; ${\bf b}$ and ${\bf c}$ show repeats of the same experiment using different pairs of mice. Error bars indicate technical variance of gPCR.





cells (top). The cells were analyzed for hydroxyurea-induced Hist1h2ak degradation (bottom) as in b. (e) Scheme of the cRT-PCR procedure. (f) RT-PCR amplification of a Hist2h4 fragment spanning the ligated 5' and 3' ends from RNA isolated from Eri1-deficient or wild-type MEF cells, either treated with TAP or left untreated before RNA ligation and RT-PCR. Amplicons are shown on a 2% agarose gel. (g) cRT-PCR sequencing results of Hist2h4 mRNA from Eri1-deficient (gray bars) and wild-type MEF cells (black bar). (h) RNA immunoprecipitation with a monoclonal antibody against Eri1, using wild-type and Eri1-deficient cells or Eri1-deficient cells reconstituted with wild-type or mutant Eri1. In a, d and f-h, representatives of at least two independent experiments are shown. In b, s.d. is calculated from three or two ('GFP-Eri1' and 'GFP') individual experiments. In a, c and d, error bars indicate qPCR variance.

Eri1 binds and trims histone mRNA in cells

(d) Expression of human Eri1 and α -tubulin in Eri1-deficient MEF

We determined the extent of Eri1 association with an endogenous histone mRNA in retrovirally reconstituted Eri1-deficient cells. Using anti-GFP immunoprecipitation, we found that Hist1h2ak mRNA coimmunoprecipitated efficiently with the catalytically inactive mutant GFP-Eri1 D130G E132G but not with GFP (Fig. 2a). We then asked whether histone mRNAs are direct targets for the catalytic activity of Eri1. Hydroxyurea treatment-induced degradation of the Hist2h4 mRNA was compared in cells that lack Eri1 alleles (Eri1-/-) or express endogenous Eri1 (Eri1+/+) or GFP-tagged Eri1 proteins (Fig. 2b,c and Supplementary Fig. 2a). Reconstitution of Eri1-deficient cells with wild-type Eri1 that was N-terminally fused to GFP was able to rescue histone mRNA degradation only partially. This result may involve a possible negative effect of the tag on Eri1 activity, but it still allowed comparison of wild-type and mutant Eri1 proteins. Histone mRNA degradation was still impaired in Eri1-deficient cells transduced to express the catalytically inactive Eri1 mutant (GFP-Eri1 D130G E132G) or GFP alone. We also addressed whether the enzyme depended on the SAP domain that has been implicated in contacting the histone mRNA stem-loop⁸. In contrast to the catalytically inactive mutant, a partial rescue of histone mRNA degradation was observed upon re-expression of an N-terminal deletion mutant (GFP-Eri1 Δ N), which lacks the SAP domain, spanning amino acids 1-106 (ref. 6). To analyze the kinetics of histone mRNA degradation in Eri1-/- MEF cells reconstituted with GFP-Eri1 and GFP-Eri1ΔN (Supplementary Fig. 2b), we determined hydroxyurea-induced Hist1h2ak mRNA decay in a time course (Fig. 2c). Again, retroviral transduction of Eri1-/- cells with wild-type GFP-Eri1 did not fully reconstitute Eri1

activity (Fig. 2c). However, the wild-type protein was more effective in *Hist1h2ak* mRNA degradation, as the GFP-Eri1ΔN mutant showed a strongly delayed mRNA decay (Fig. 2c). Nevertheless, 60 min after hydroxyurea treatment, GFP-Eri1∆N decreased *Hist1h2ak* mRNA to a similar extent as GFP-Eri1 (Fig. 2c).

Sequencing frequency (%)

Because previous knockdown approaches were unable to demonstrate a function for human ERI1 in hydroxyurea-induced histone mRNA degradation²⁰, we also addressed the possibility of mouse and human ERI1 proteins serving a different function. Similar to the function of endogenous mouse Eri1 protein, the Flag-HA-tagged human counterpart clearly rescued hydroxyurea-induced degradation of *Hist1h2ak* in Eri1-deficient cells (**Fig. 2d**).

Our previous work showed that the 3' exoRNase activity of Eri1 was essential for trimming the 3' end of 5.8S rRNA⁶. This prompted us to inspect the 3' end of the *Hist2h4* mRNA in wild-type and Eri1-deficient cells by circularization reverse transcription PCR (cRT-PCR)²⁰ (**Fig. 2e**). In this method, the 3' and 5' ends of an individual RNA molecule are ligated to form a circle, which is followed by reverse transcription and PCR amplification across the joined ends. We found that cRT-PCR amplification of Hist2h4 required treatment of RNA samples with tobacco acid pyrophosphatase (TAP) (**Fig. 2f**), an enzyme that removes the cap structure at the 5' end of mRNA molecules. In these TAPtreated mRNAs, we compared the Hist2h4 mRNA 3' ends of five wildtype clones with those of nine clones derived from Eri1-deficient cells. The sequences clearly showed that the presence of the Eri1 wild-type allele correlated with trimming of the last two nucleotides of the AACCA sequence at the 3' end of the Hist2h4 mRNA (Fig. 2g). In fact, it created a 3' end that was similar to the previously determined

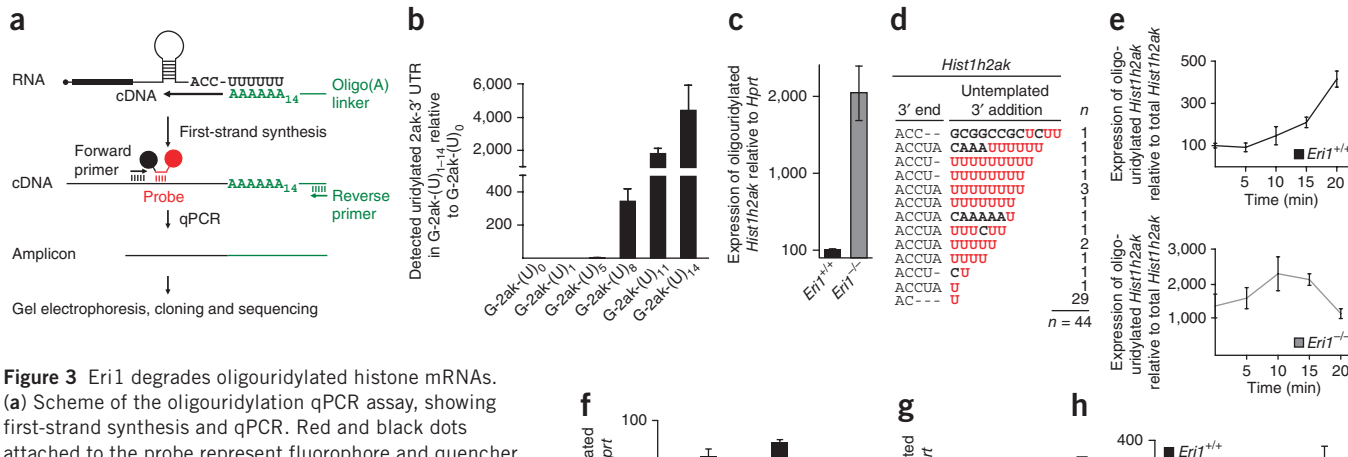
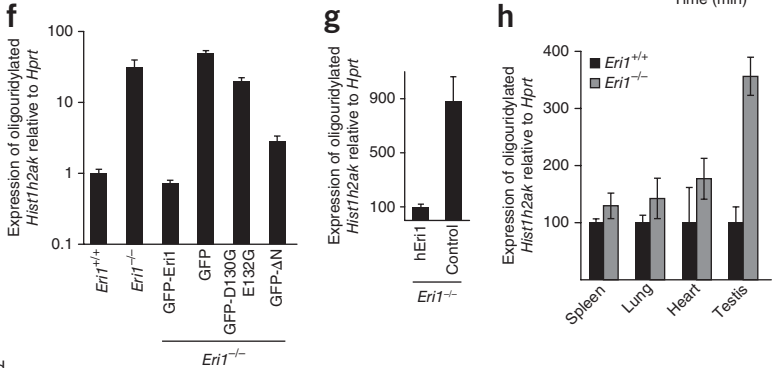


Figure 3 Eri1 degrades oligouridylated histone mRNAs.

(a) Scheme of the oligouridylation qPCR assay, showing first-strand synthesis and qPCR. Red and black dots attached to the probe represent fluorophore and quencher, respectively. (b) Electroporation of wild-type MEF cells with in vitro transcribed mRNAs. Constructs have the Hist1h2ak 3' UTR fused to the open reading frame of GFP with increasing numbers of Us at their 3' end (G-2ak-(U)₀₋₁₄) (Supplementary Fig. 4). Total RNA was prepared 24 h after transfection. To measure levels of uridylated Hist1h2ak relative to GFP, the detection of both mRNAs was normalized to that of Hprt, as GFP cannot be measured in the oligouridylation assay. The ratio was calculated (G-2ak-(U)₁₋₁₄/G-2ak-(U)₀). (c) Quantification of oligouridylated Hist1h2ak mRNA in asynchronously growing Eri1-deficient and wild-type MEF cells. (d) Analysis of uridylated



3' ends of endogenous *Hist1h2ak* in Eri1-deficient MEF cells, with ligation of a linker to the 3' end of gel-purified RNAs (~200–800 nucleotides). For reverse transcription, a primer with the complementary linker sequence and a 3' anchoring A was used. Uridylated *Hist1h2ak* was amplified with a forward primer annealing at the 3' UTR and a reverse primer in the linker region. PCR fragments were cloned and sequenced. (e-h) PCR quantification of oligouridylated *Hist1h2ak* mRNA in wild-type and Eri1-deficient MEF cells in response to hydroxyurea treatment (e), in mRNA from samples shown in **Figure 2b** and **Supplementary Figure 5** (f) and in samples from **Figure 2d** (g) or in mRNA extracted from tissues of Eri1-deficient and wild-type mice (h). c and e-h are representative of at least two independent experiments, and d combines results from three independent experiments. Error bars in b,c and e-h indicate technical variance of qPCR.

3′ end of histone HIST2H3 mRNAs in HeLa cells²⁰. Eri1 deficiency instead led to mRNA molecules that terminated either four (AACC) or five (AACCA) nucleotides downstream of the stem-loop (**Fig. 2g**), which were similarly found for histone H2a mRNA when processing occurred *in vitro*²⁰.

The five nucleotides of the consensus sequence ACCCA at the 3' end of replication-dependent histone mRNAs have been found to be crucial for the interaction of recombinant Eri1 with short oligoribonucleotides that form the stem-loop structure in solution. Shortening or extension, as well as replacement with an AUUUU sequence, reduced the interaction of recombinant Eri1 significantly⁸. Having established that Hist2h4 mRNA, in the presence of catalytically active Eri1, ends in an AAC sequence, we tested whether 3'-end trimming would abolish the association of Eri1 with the histone mRNA. We performed anti-Eri1 RNA immunoprecipitations (RIPs) after formaldehyde cross-linking of intact cells⁶. In these experiments, we found that endogenous Eri1 from wild-type cells and Eri1 that was re-expressed in Eri1-deficient cells were equally able to interact with Hist2h4 mRNA (Fig. 2h). Efficient binding was also observed for the catalytically inactive mutant of Eri1 (GFP-Eri1 D130G E132G) (Fig. 2h). In contrast, no binding was observed in immunoprecipitations from Eri1-deficient cells transduced with empty vector or transduced with Eri1 harboring two mutations (K107A K108A) that were previously shown to interfere in human ERI1 with histone mRNA binding⁸. A naturally occurring polymorphism of mouse Eri1 with one amino acid substitution (A176D)⁶ did not interfere with histone mRNA binding. These data suggest that Eri1 interaction with the

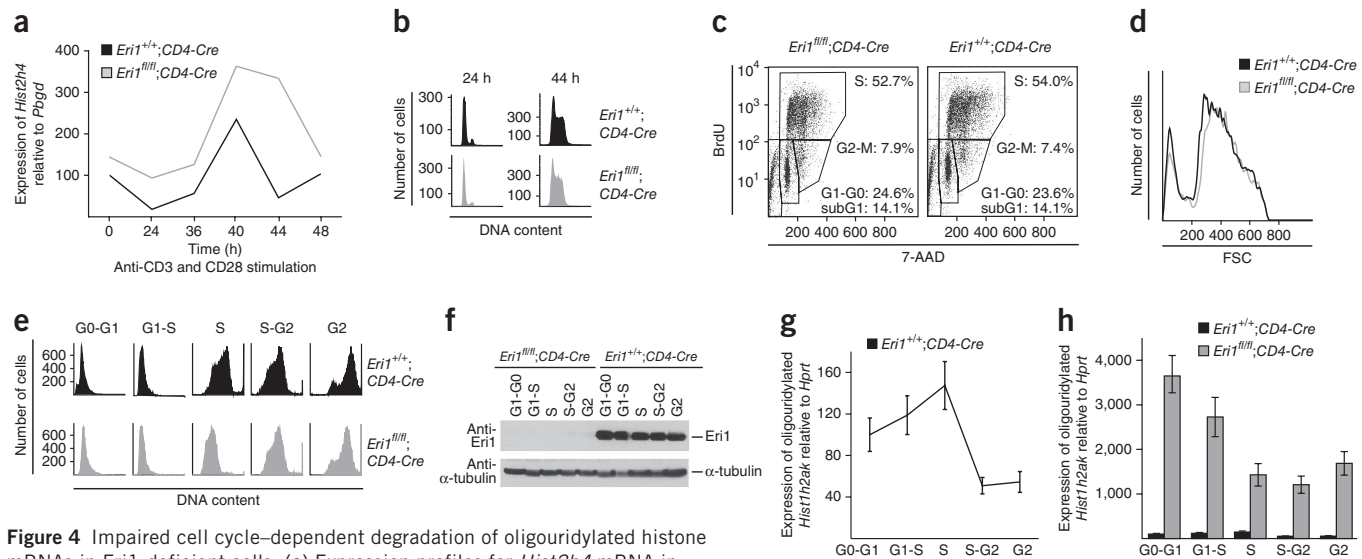
histone mRNA may be stabilized by other proteins, for example by SLBP as previously described⁸ or by *cis* elements other than the consensus ACCCA motif. The findings also show that the Eri1 protein trims two nucleotides from the mature histone mRNA 3' end but then stalls close to the double-stranded stem-loop structure.

Oligouridylated histone mRNAs accumulate upon Eri1 deficiency

Addition of nontemplated oligo(U) tails to the 3' end of histone mRNAs has been implicated as the degradation-initiating event²⁰. We set up an assay to quantify these short-lived oligo(U)-marked histone mRNAs, performing reverse transcription under optimized conditions with a primer that included 14 As (Fig. 3a and Supplementary Fig. 3a). To validate how many Us have to be present at the 3' end of the histone mRNA to be detected, the assay was tested on in vitrotranscribed uridylated and oligouridylated transcripts after electroporation into MEF cells. It was possible to detect the 3' untranslated region (UTR) of Hist1h2ak fused to GFP mRNA (Supplementary Fig. 4) when it was extended by more than five Us (Fig. 3b). However, the efficiency of detection steeply increased between 5 and 14 Us. In asynchronously growing cells, the detection of endogenous oligouridylated *Hist1h2ak* increased by a factor of ~20 in Eri1-deficient as compared to wild-type cells (Fig. 3c). We then ligated RNA linkers to RNA from Eri1-deficient cells and used a linker-specific primer, which anchored the reverse transcription to templates that ended in at least one U. For *Hist1h2ak* transcripts that ended in the sequences ACCUA or ACCU, which were found appropriate for Eri1-deficient cells (Fig. 2g), we determined uridylation to involve additions of







mRNAs in Eri1-deficient cells. (a) Expression profiles for Hist2h4 mRNA in Eri1-deficient and wild-type CD4 T cells, determined by qPCR. Samples are from peripheral CD4 T cells isolated from wild-type and Eri1-targeted mice, as indicated and activated with anti-CD3 and anti-CD28 antibodies to enter the cell cycle. The experiment was performed five times, measuring Hist2h4 in four and Hist1h1a, Hist1h1e and Hist1h2ak in one experiment(s). In all experiments, histone mRNA expression was significantly increased in Eri1-deficient cells after 40 h, as determined by the paired Student's t-test (P = 0.03 for Hist2h4). (b) Propidium iodide staining and fluorescenceactivated cell sorting (FACS) analysis of samples in a. (c,d) Cell cycle (c) and size (d) analysis of T_H2 cells from wild-type and Eri1-deficient mice.

BrdU, bromodeoxyuridine; 7-AAD, 7-aminoactinomycin D. (e-h) Centrifugal elutriation of Eri1-deficient and wild-type T_H2 cells. The different cellcycle phases were identified through their DNA contents in propidium iodide staining and FACS analysis (e). (f-h) Protein or RNA extracts analyzed by immunoblotting using an anti-Eri1 monoclonal antibody (f) or qPCR for oligouridylation of histone Hist1h2ak (g,h). g and h depict the same data for wild-type T_H2 cells that are directly compared to oligouridylation levels of Hist1h2ak in Eri1-deficient cells in h. c-h are representative of two experiments. Error bars in ${\bf g}$ and ${\bf h}$ indicate technical variance of qPCR.

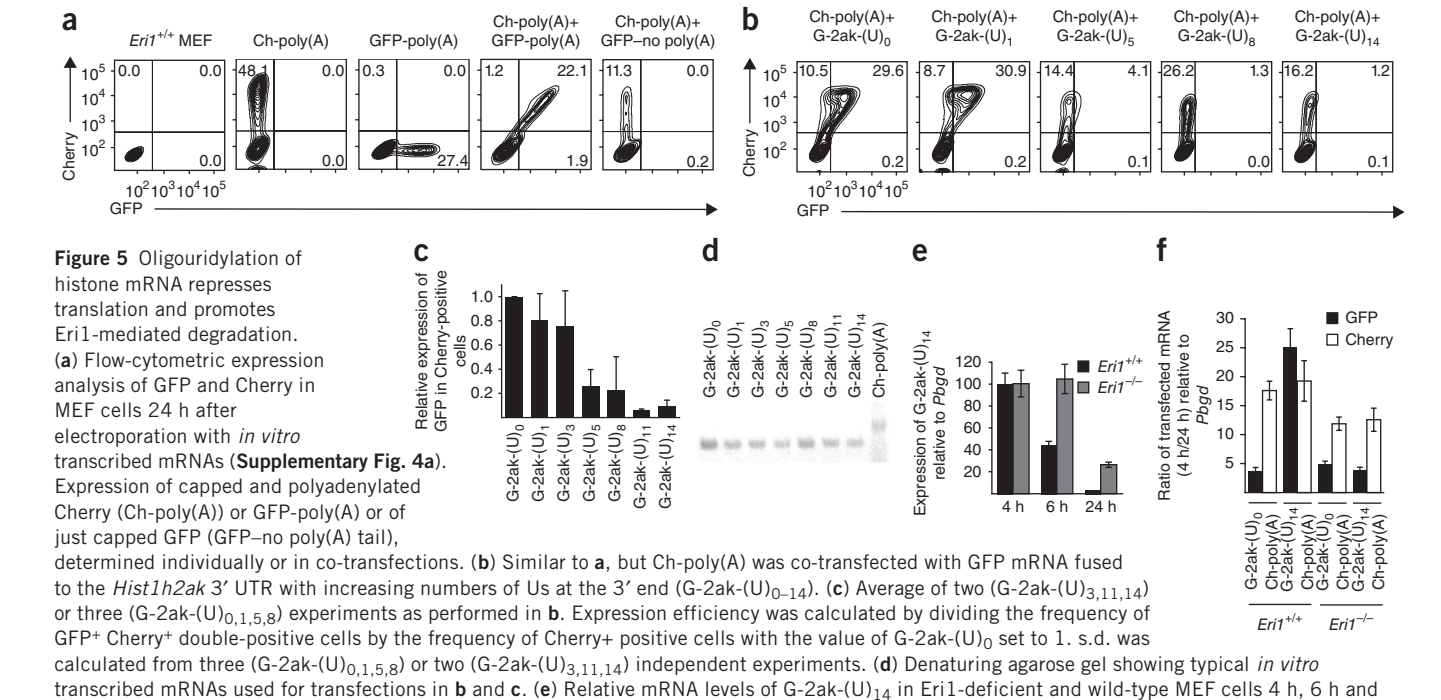
1-9 Us as well as 3' additions of CAAAAAU or CAAAUUUUUU (Fig. 3d). Unexpectedly, we also found *Hist1h2ak* transcripts that were shortened by 3 nucleotides in the absence of Eri1. These transcripts were 3' monouridylated, which suggested that this type of modification occurs in association with 3'-end degradation.

Hydroxyurea treatment induced a steady increase of oligouridylation of *Hist1h2ak* mRNA over 20 min in wild-type MEF cells (Fig. 3e). Eri1-deficient MEF cells responded only marginally after 10 min (Fig. 3e), but oligouridylation in these cells was elevated at all time points by more than one order of magnitude, compared to wild-type cells. We then tested whether re-expression of GFP-Eri1 could rescue this phenotype in Eri1-deficient MEF cells. In these experiments, GFP-Eri1 completely reduced oligouridylation of Hist1h2ak mRNA to wildtype levels, whereas the catalytically inactive GFP-Eri1 D130G E132G mutant was ineffective (Fig. 3f and Supplementary Fig. 5). This rescue activity was not restricted to mouse Eri1 but also occurred upon reconstitution with human ERI1 (Fig. 3g). Much as we had observed after hydroxyurea-induced histone mRNA degradation (Fig. 2b,c), we found that the RNA-binding mutant GFP-Eri1∆N partially rescued *Hist1h2ak* oligouridylation levels (**Fig. 3f** and **Supplementary Fig. 5**). The increased abundance of oligouridylated histone mRNAs was also confirmed in RNA samples prepared from tissues of Eri1-deficient and wild-type mice (Fig. 3h). These measurements showed smaller differences in organs composed mainly of cells that are resting or are terminally differentiated (Fig. 3h, spleen, lung and heart). However, a greater difference was detected in the mRNA samples prepared from testis (Fig. 3h), consistent with the fact that many cells are progressing in the cell cycle in this organ. These results demonstrate that the exonucleolytic activity of Eri1 decreased the abundance of oligouridylated histone mRNAs, whereas the intrinsic RNA-binding capacity of Eri1 was dispensable.

Eri1-deficient cells progress normally in the cell cycle

To find out how the apparent defect of Eri1-deficient cells can be compensated for in the cell cycle, we performed time-course experiments to measure histone mRNA expression in quasisynchronized cells by activating naive CD4 T cells with anti-CD3 and anti-CD28 antibodies (Fig. 4a,b). This treatment similarly induced Eri1-deficient and wild-type cells to leave the G0 phase and to enter and progress in the cell cycle (Fig. 4b). Hist2h4 mRNA expression profiles in Eri1deficient and wild-type cells were comparable in that they increased after 24 h of stimulation, peaked after 40 h and subsequently declined to basal levels after 48 h or 44 h, respectively (Fig. 4a). Over all time points the Hist2h4 mRNA abundance in Eri1-deficient cells was slightly increased. However, the decay of histone mRNA was delayed 40-44 h after stimulation as compared to wild-type cells (Fig. 4a). At that time, both samples exhibited similar cell-cycle progression, as determined by DNA-content analysis (Fig. 4b). Still, histone mRNA degradation was eventually achieved. These data suggest that Eri1deficient T cells implement an alternative but slower histone mRNA degradation pathway within their cell cycle, which was not obvious during short-term hydroxyurea treatment. To formally rule out effects of Eri1 deletion on the cell cycle of T cells, we performed bromodeoxyuridine (BrdU) incorporation experiments after culturing the cells 3 d in T_H2 conditions. Analyzing asynchronously growing wild-type and Eri1-deficient T cells, we found no differences in the distribution of cells in sub G1, G0-G1, S or G2-M phase (Fig. 4c) and no difference in cell size (Fig. 4d).

In order to analyze oligouridylation in individual cell-cycle phases, we employed centrifugal elutriation to separate fractions of wild-type and Eri1-deficient T cells. These were judged by their DNA content to represent cells mostly in G0-G1, G1-S, S, S-G2 and G2 phases (Fig. 4e). Eri1-deficient and wild-type T cells were close



24 h after transfection. (f) Eri1-deficient and wild-type MEF cells, co-transfected with G-2ak(U)₀ and Ch-poly(A) or G-2ak-(U)₁₄ and Ch-poly(A) to determine the ratio of either GFP or Cherry between 4 h and 24 h after transfection. e and f are representative of two independent experiments.

to identical in their DNA content, with the exception of the S-phase elutriation fraction that, owing to unknown reasons, showed slightly less DNA content in the Eri1-deficient cells. Immunoblotting of T-cell lysates derived from the same cell fractions did not reveal obvious regulation of the Eri1 protein in the wild-type cells during the cell cycle (**Fig. 4f**). We then compared the dynamics of oligouridylation of *Hist1h2ak* during cell-cycle progression in T cells. In wild-type T cells, oligouridylation of *Hist1h2ak* increased from G1 over G1-S to late S phase and decreased in S-G2 phase (**Fig. 4g**). The total amount of *Hist1h2ak* increased as expected from G0-G1 to early S phase and continuously decreased toward G2-M phase

Error bars indicate technical variance of gPCR.

(Supplementary Fig. 6a). Oligouridylation of *Hist1h2ak* in Eri1-deficient T cells was increased throughout the cell cycle and was highest in G1 phase, with strongly increased levels as compared to wild-type cells. The levels dropped slightly during G1-S phase, S phase and S-G2 phase and increased again during the G2 phase (Fig. 4h). Nevertheless, oligouridylation of *Hist1h2ak* increased in S phase when we normalized to the total amount of *Hist1h2ak* (Supplementary Fig. 6b), which suggested a higher activity of the responsible cellular TUTase during this cell-cycle phase. These findings implicate the existence of an Eri1-independent pathway to degrade oligouridylated histone mRNAs.

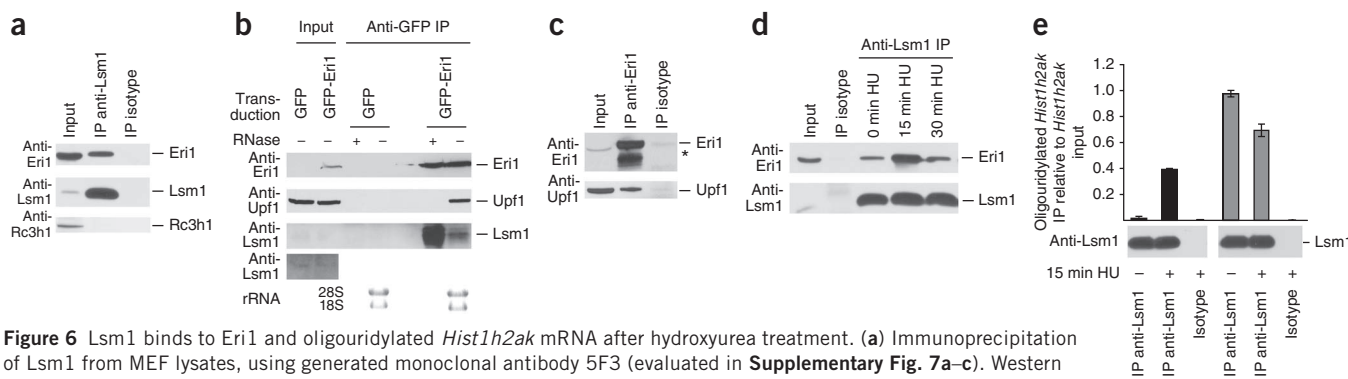


Figure 6 Lsm1 binds to Eri1 and oligouridylated *Hist1h2ak* mRNA after hydroxyurea treatment. (a) Immunoprecipitation of Lsm1 from MEF lysates, using generated monoclonal antibody 5F3 (evaluated in **Supplementary Fig. 7a–c**). Western blot analysis using a second monoclonal antibody (2A8) to detect Lsm1 is shown. Additionally, co-immunoprecipitation of Eri1 but not Rc3h1, another RNA binding protein, was observed. (b) Anti-GFP immunoprecipitations on cell lysates from Eri1-deficient MEF cells retrovirally transduced with GFP-Eri1 or GFP alone, that were treated with a mixture of

RNases or left untreated. The indicated proteins were detected by immunoblotting. The Lsm1 protein in the input was detected only upon prolonged exposure. Effective RNase treatment was demonstrated through ethidium bromide staining of the 28S and 18S rRNA bands after RNA-extraction of immunoprecipitation supernatants. (c) Immunoprecipitation of endogenous Eri1 from CD4 T cell lysates, using a monoclonal Eri1 antibody. Eri1 and Upf1 were detected by immunoblotting. Asterisk denotes a degradation product of Eri1. (d) Immunoprecipitation performed as in a, but MEF cells were treated with hydroxyurea for 0, 15 or 30 min. (e) Similar to d, but anti-Lsm1 immunoprecipitates were washed with a high-salt buffer that efficiently disrupts Lsm1-Eri1 interactions. Half of each immunoprecipitated sample was analyzed by western blot or qPCR for oligouridylated *Hist1h2ak*. In a–e, experiments were performed at least twice. Error bars in e indicate the technical variance of the qPCR results.

78



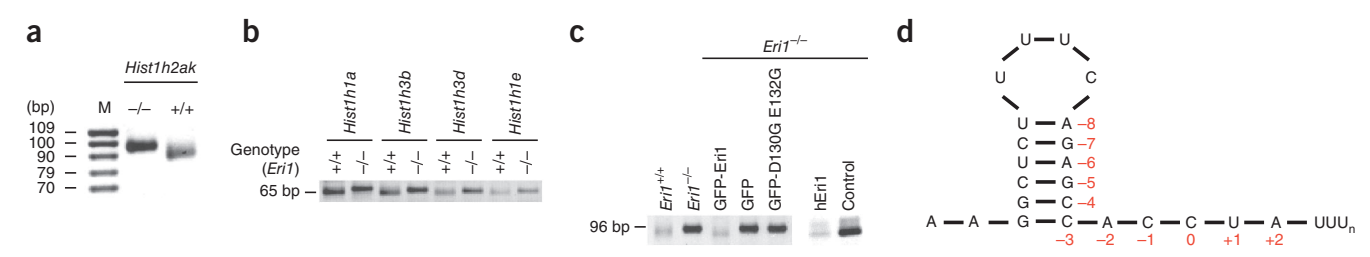
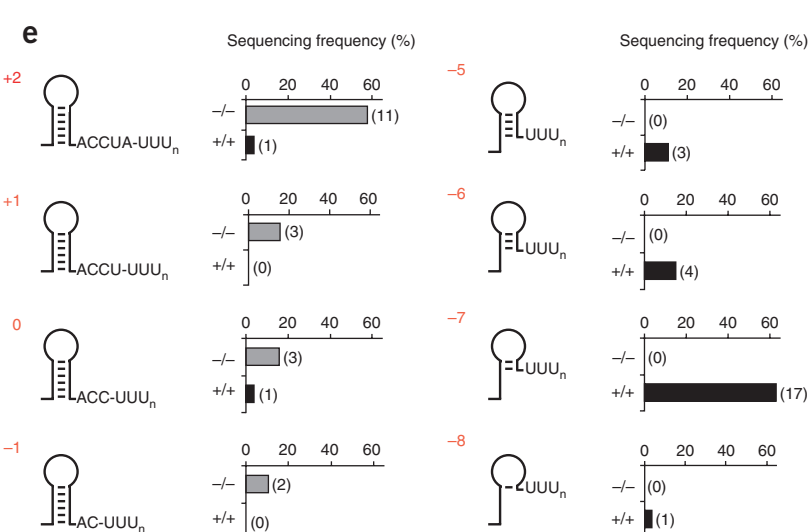


Figure 7 Eri1 degrades through the stem-loop in consecutive cycles of oligouridylation and partial degradation. (a) Oligouridylated Hist1h2ak PCRamplification products derived from cDNA of wild-type or Eri1-deficient MEF cells, separated on a 4% agarose gel. (b) Oligouridylated Hist1h1a, Hist1h3b, Hist1h3d and Hist1h1e amplified and analyzed as in a. (c) Oligouridylated Hist1h2ak amplified from cDNA of Eri1-deficient MEF cells retrovirally transduced with GFP, GFP-Eri1, hEri1 or the catalytically inactive Eri1 mutant GFP-D130G E132G and analyzed as in a. (d) Schematic representation of the Hist1h2ak mRNA stem-loop. Red numbers were allocated to different stages of mRNA decay. (e) Stages of stem-loop decay illustrated for oligouridylated Hist1h2ak PCR-amplification products cloned and sequenced from 27 wild-type clones and 19 clones derived from Eri1-deficient cells. Numbers refer to those in d. Representative gel images from at least two independent experiments are shown in a and c; e summarizes data from two independent experiments.



Eri1 degrades histone mRNAs in their oligouridylated form

We determined the protein expression and half-life of oligouridylated histone mRNAs in wild-type and Eri1-deficient MEF cells. To do so, we performed transfections of in vitro-transcribed and 5'-capped mRNAs encoding the open reading frame of GFP fused to the 3' UTR of Hist1h2ak (G-2ak) (Supplementary Fig. 4). As an internal control, we also cloned and in vitro transcribed polyadenylated Cherry mRNA (Ch-poly(A)). Single and double mRNA transfections revealed that both fluorescent proteins were efficiently expressed if equipped with a poly(A) tail (Fig. 5a). Expression of GFP with a stem-loop was reduced as compared to that of the same mRNA ending in a poly(A) tail (Fig. 5a,b). We then analyzed the influence of increasing numbers of Us added to the 3' end of the Hist1h2ak 3' UTR (G-2ak-(U)₀₋₁₄) (Fig. 5b). In these experiments, we found no effect on GFP expression upon addition of one or three Us to the 3' end of the Hist1h2ak 3' UTR (Fig. 5b-d). In contrast, 5-14 Us reduced or blocked GFP expression in most of the transfected cells. In fact, green fluorescence was undetectable for cells that received mRNAs ending in 11-14 Us and was similar to transfections of a GFP transcript with no poly(A) tail (Fig. 5a,b).

Next we asked whether oligouridylation influenced histone mRNA stability in wild-type and Eri1-deficient cells. The mRNA levels of the oligouridylated reporter (G-2ak(U)₁₄) declined much faster at 6 h and 24 h in wild-type compared to Eri1-deficient cells (Fig. 5e). In contrast, the decrease of the nonuridylated reporter was similar in both cell lines (Fig. 5f; G-2ak-(U)₀). The degradation of co-transfected Cherry mRNA was also comparable (Fig. 5f, Ch-poly(A)). These data show that only the oligouridylated form of *Hist1h2ak* is a target for Eri1-dependent degradation and suggest that oligouridylation interferes with protein expression.

Eri1 interacts with Lsm1, Lsm4 and Upf1 proteins

We hypothesized that Eri1 may act on oligouridylated mRNAs in concert with Lsm1 and Upf1 proteins, which are required for

replication-dependent histone mRNA decay^{20,22,26}. To analyze the interaction of Eri1 with Lsm1, we generated monoclonal antibodies against Lsm1 (Supplementary Fig. 7a-c). Immunoprecipitating endogenous Lsm1 from wild-type MEF cell extracts, we found substantial co-immunoprecipitation of Eri1 (Fig. 6a). The interaction was specific, as Rc3h1, another RNA-binding protein²⁷ was not coimmunoprecipitated with Lsm1, and no Eri1 signal appeared in an isotype-control immunoprecipitation. We also confirmed this interaction through Eri1 pulldowns. Here, we performed immunoprecipitations with antibodies against GFP, using extracts of Eri1-deficient MEF cells transduced with retroviruses expressing either GFP or GFP-Eri1 (Fig. 6b). Again, immunoprecipitation of GFP-Eri1 but not GFP revealed an interaction with endogenous Lsm1 (Fig. 6b). Similarly, immunoprecipitation of Eri1 from extracts of T cells revealed an interaction with the helicase Upf1 (Fig. 6c).

We then asked whether any of these interactions occurred in the absence of RNA. Immunoprecipitations were performed with cell lysates that were either left untreated or supplemented with RNase (Fig. 6b). Upf1 was co-immunoprecipitated only when RNA was present, as the signal was lost upon RNase-treatment (Fig. 6b). This indicated that these two proteins were present in the same messenger ribonucleoprotein complex but did not engage in proteinprotein interactions. In contrast, Eri1 interacted with Lsm1, and the western blot signal even increased when RNase was added to the cell lysate (Fig. 6b). RNase treatment in this case may liberate Lsm complexes from nonhistone mRNAs, making them more accessible for binding Eri1 in the lysates. This conclusion was supported by co-immunoprecipitation of Lsm4 protein with endogenous Eri1 from T-cell lysates in which RNase treatment also strongly enhanced endogenous Eri1 interaction with endogenous Lsm4 (Supplementary Fig. 7d). These results point toward an RNase-insensitive interaction of Eri1 with one or several members of the heteroheptameric Lsm1-7 ring, which is known to specifically bind oligouridylated or



oligoadenylated mRNAs^{23,28}. In line with this, we found that the interaction of Eri1 with Lsm1 in extracts of wild-type MEF cells transiently increased 15 min after hydroxyurea treatment (**Fig. 6d**). At this time point, we also found more oligouridylated histone *Hist1h2ak* mRNA in anti-Lsm1 RNA immunoprecipitations (**Fig. 6e**). Notably, Lsm1 interaction with this histone mRNA was not dependent on the presence of Eri1 and rather appeared increased in the Eri1-deficient cells, even before hydroxyurea treatment. This is consistent with increased basal levels of oligouridylated transcripts in these cells (**Fig. 3c**). The results therefore support a model in which Eri1 may gain specificity for the degradation of oligouridylated histone mRNAs through its interaction with Lsm1–7 proteins.

Eri1 degrades the stem-loop of oligouridylated histone mRNAs

We repeatedly noticed that PCR amplicons of oligouridylated histone mRNAs from Eri1-deficient and wild-type MEF cell extracts ran differently in gel electrophoresis (Fig. 7a-c). The wild-type band migrated somewhat faster and appeared diffuse. We detected similar differences in band size between Eri1-deficient and wild-type MEF cells for amplicons of oligouridylated Hist1h1a, Hist1h3b, Hist1h3d and *Hist1h1e* (**Fig. 7b**). Furthermore, retroviral transduction of mouse or human ERI1 in Eri1-deficient MEF cells converted the slowermigrating and more defined band that is characteristic for Eri1deficient cells into a faster-running and more diffuse wild-type band (Fig. 7c). The phenotype could not be rescued by the catalytically inactive mutant GFP-Eri1 D130G E132G (Fig. 7c). Sequences from 27 clones originating from wild-type MEF mRNA showed that oligouridylation was hardly present at the 3' end of mature Eri1-trimmed Hist1h2ak mRNA. Instead, oligouridylation was almost entirely found at 3' ends of mRNAs that showed intermediate degradation into the stem-loop (93%). These stages are depicted and were designated +2 to -8 with respect to position 0 being the 3' end of mature Eri1-trimmed Hist1h2ak (Fig. 7d). The oligouridylated 3' end at position -7 was by far the most abundantly occurring oligouridylated degradation product in wild-type MEF cells (62%) (Fig. 7e). These results strongly indicate that oligouridylated full-length histone mRNAs are rapidly degraded into the stem-loop, where degradation stalls, and that full degradation of the stem-loop requires re-oligouridylation. In sharp contrast to these findings, oligouridylation of Hist1h2ak in Eri1-deficient MEF cells was not found at the 3' end of transcripts with a partially degraded stem-loop, that is, with 3' ends below the -1 position. Instead, oligouridylation of Hist1h2ak mRNA in Eri1-deficient cells was mostly found at position +2 (Fig. 7e), that is, on full-length mRNA that lacked Eri1-dependent 3'-end trimming (58%).

DISCUSSION

We demonstrated the crucial role of Eri1 in histone mRNA degradation, representing one paradigm of induced mRNA decay. We observed Eri1-dependent trimming of two nucleotides at the 3' end of mature histone *Hist2h4* mRNA (**Fig. 2g**). This is consistent with previous observations describing that cytoplasmic mature histone mRNAs are two nucleotides shorter than those processed in *in vitro* reactions that lack Eri1 (ref. 20). *In vitro*, the Eri1 protein shortened the 3' end of histone mRNAs by 2–3 nucleotides at limiting concentrations and progressively degraded the mRNA at higher protein concentrations⁷. Such nonspecific degradation was inhibited in the presence of the SLBP protein⁷. However, trimming of histone mRNAs by Eri1 can also be interpreted as an unsuccessful attempt at 3'-end degradation, which requires oligouridylation to become effective (**Fig. 5e**). This inhibition could be due to steric constraints or to the double-stranded RNA structure of the stem-loop, which is known

to inhibit Eri1 exoRNase activity in vitro^{1,6,7}. According to a previous report, Eri1 binding to the stem-loop required the full ACCCA at the 3' end⁷. Therefore, Eri1-mediated trimming could destabilize its own binding for subsequent degradation of the stem-loop, unless additional interaction surfaces are created in an oligouridylated histone messenger ribonucleoprotein complex. The Lsm1-7 complex binds 3'-oligouridylated transcripts, and we found that Eri1 interacts in cell lysates in an RNA-independent and hydroxyurea-inducible manner with the Lsm1 complex (Fig. 6a,d). We also found that Eri1 co-immunoprecipitated with Upf1 in an RNase-sensitive manner (Fig. 6b,c). Previous publications have shown that SLBP interacted directly with Upf1 (ref. 22) and, in an RNase-sensitive manner, with Lsm1 (ref. 20), and both interactions were stimulated by hydroxyurea^{20,22}. Considering the inhibition of Eri1 catalytic activity by RNA duplexes, the Eri1-Lsm1-7 complex may be able to process through the stem-loop only when the helicase activity of Upf1, presumably in a stepwise manner, opens up the double-stranded RNA of the stem. This scenario would provide a mechanistic interpretation for the functional importance of Upf1 in this pathway^{20,22}.

It was previously shown that binding of the Lsm1-7 complex to oligo(U) tails can cause decapping of mRNAs^{28,29}. The same function of Lsm1 was recently proposed in the process of histone mRNA degradation²⁰. Experimental evidence included the detection of 5'-shortened transcripts after circularization PCR as well as the knockdown of Dcp2, which resulted in a two-fold reduction of hydroxyurea-induced histone mRNA degradation²⁰. Our data show that oligouridylation of full-length histone mRNAs is profoundly increased in Eri1-deficient cells (Fig. 3c and Fig. 4h), and hydroxyurea treatment induces only a modest reduction of histone mRNAs (Fig. 1a-c). We therefore consider decapping as an alternative degradation pathway in wild-type cells. We can also not rule out involvement of 3' degradation by the exosome²⁰, although a previous publication described that oligouridylation interfered with 3'-5' degradation in cell extracts²⁹. However, these alternative pathways are much less effective in Eri1-deficient cells. We also determined that oligouridylated transcripts are translationally repressed (Fig. 5c), which could result from Lsm1-7 binding, as translational inhibition has been found to be associated with the binding of activators of mRNA decapping³⁰. Translational inhibition together with alternative degradation may prevent the development of signs of genomic instability due to histone overexpression in Eri1deficient mice. Nevertheless, the increased abundance and delayed decay of histone mRNAs due to Eri1 deficiency may cause problems under certain circumstances, for example in rapidly growing cells during an ongoing immune response⁴ or in processes that require replacement with specific histone variants.

The untemplated addition of Us to the 3' end of RNAs by TUTases was observed for several RNA classes, the U6 (ref. 31), miRNAs^{32,33} and histone mRNAs²⁰, but the mechanistic implications of this modification are not well understood. For the let-7 family of miRNAs, it was shown that lin28 binds sequence specifically to the loop of pre-let-7 miRNAs and recruits the TUTase Zcchc11 for oligouridylation³⁴. This renders pre-let-7 no longer a substrate for Dicer processing³². Consequently, no mature let-7 is produced, but the fate of oligouridylated pre-let-7 is unknown. Because we showed that Eri1 is an exonuclease that selectively degrades oligouridylated histone mRNAs, we speculate that the range of potential substrates might not be restricted to the class of histone mRNAs.

METHODS

Methods and any associated references are available in the online version of the paper. ACKNOWLEDGMENTS

Note: Supplementary information is available in the online version of the paper.

We would like to thank W. Pastor and A. Rao (La Jolla Institute of Allergy and Immunology, La Jolla, CA, USA) for providing the FLAG-HA-hERI1 construct. We thank D. Repsilber (Leibniz Institute for Farm Animal Biology, Dummerstorf, Germany) for advice on statistical analyses. R. Lührmann (Max Planck Institute for Biophysical Chemistry, Göttingen, Germany) kindly provided anti-Lsm1 antibodies. This work was supported by the German Research Foundation (DFG HE 3359/3-1 to V.H.).

AUTHOR CONTRIBUTIONS

V.H. and K.M.A. conceived of the project idea. K.P.H. and V.H. designed and K.P.H. performed most of the experiments with help from C.W., J.D. and A.S. N.R. carried out the reconstitution experiments. N.R. and G.A.H. performed the immunoprecipitation experiments, and E.K. generated the monoclonal antibodies. K.P.H., V.H. and K.M.A. discussed the data, and K.P.H. and V.H. wrote the manuscript.

COMPETING FINANCIAL INTERESTS

The authors declare no competing financial interests.

Published online at http://www.nature.com/doifinder/10.1038/nsmb.2450. Reprints and permissions information is available online at http://www.nature.com/ reprints/index.html.

- Kennedy, S., Wang, D. & Ruvkun, G. A conserved siRNA-degrading RNase negatively regulates RNA interference in C. elegans. Nature 427, 645-649 (2004).
- lida, T., Kawaguchi, R. & Nakayama, J. Conserved ribonuclease, Eri1, negatively regulates heterochromatin assembly in fission yeast. Curr. Biol. 16, 1459-1464 (2006).
- Bühler, M., Verdel, A. & Moazed, D. Tethering RITS to a nascent transcript initiates RNAi- and heterochromatin-dependent gene silencing. Cell 125, 873-886
- Thomas, M.F. et al. Eril regulates microRNA homeostasis and mouse lymphocyte development and antiviral function. Blood 120, 130-142 (2012).
- Gabel, H.W. & Ruvkun, G. The exonuclease ERI-1 has a conserved dual role in 5.8S rRNA processing and RNAi. Nat. Struct. Mol. Biol. 15, 531-533 (2008).
- 6. Ansel, K.M. et al. Mouse Eri1 interacts with the ribosome and catalyzes 5.8S rRNA processing. Nat. Struct. Mol. Biol. 15, 523-530 (2008).
- Dominski, Z., Yang, X.C., Kaygun, H., Dadlez, M. & Marzluff, W.F. A 3' exonuclease that specifically interacts with the 3' end of histone mRNA. *Mol. Cell* 12, 295–305 (2003).
- Yang, X.C., Purdy, M., Marzluff, W.F. & Dominski, Z. Characterization of 3'hExo, a 3' exonuclease specifically interacting with the 3' end of histone mRNA. J. Biol. Chem. 281, 30447-30454 (2006).
- Battle, D.J. & Doudna, J.A. The stem-loop binding protein forms a highly stable and specific complex with the 3' stem-loop of histone mRNAs. RNA 7, 123-132
- 10. Martin, F., Michel, F., Zenklusen, D., Muller, B. & Schumperli, D. Positive and negative mutant selection in the human histone hairpin-binding protein using the yeast three-hybrid system. Nucleic Acids Res. 28, 1594-1603 (2000).
- 11. Williams, A.S. & Marzluff, W.F. The sequence of the stem and flanking sequences at the 3' end of histone mRNA are critical determinants for the binding of the stem-loop binding protein. Nucleic Acids Res. 23, 654-662 (1995).

- 12. Yang, X.C., Torres, M.P., Marzluff, W.F. & Dominski, Z. Three proteins of the U7specific Sm ring function as the molecular ruler to determine the site of 3'-end processing in mammalian histone pre-mRNA. Mol. Cell. Biol. 29, 4045-4056 (2009).
- 13. Marzluff, W.F., Gongidi, P., Woods, K.R., Jin, J. & Maltais, L.J. The human and mouse replication-dependent histone genes. Genomics 80, 487-498 (2002).
- 14. Meeks-Wagner, D. & Hartwell, L.H. Normal stoichiometry of histone dimer sets is necessary for high fidelity of mitotic chromosome transmission. Cell 44, 43-52
- 15. Graves, R.A., Pandey, N.B., Chodchoy, N. & Marzluff, W.F. Translation is required for regulation of histone mRNA degradation. Cell 48, 615-626 (1987).
- 16. Pandey, N.B. & Marzluff, W.F. The stem-loop structure at the 3' end of histone mRNA is necessary and sufficient for regulation of histone mRNA stability. Mol. Cell. Biol. 7, 4557-4559 (1987).
- 17. Parker, R. & Song, H. The enzymes and control of eukaryotic mRNA turnover. Nat. Struct. Mol. Biol. 11, 121-127 (2004).
- 18. Tharun, S. & Parker, R. Targeting an mRNA for decapping: displacement of translation factors and association of the Lsm1p-7p complex on deadenylated yeast mRNAs. Mol. Cell 8, 1075-1083 (2001).
- 19. Wang, Z. & Kiledjian, M. Functional link between the mammalian exosome and mRNA decapping. Cell 107, 751-762 (2001).
- 20. Mullen, T.E. & Marzluff, W.F. Degradation of histone mRNA requires oligouridylation followed by decapping and simultaneous degradation of the mRNA both 5' to 3' and 3' to 5'. Genes Dev. 22, 50-65 (2008).
- 21. Kaygun, H. & Marzluff, W.F. Regulated degradation of replication-dependent histone
- mRNAs requires both ATR and Upf1. Nat. Struct. Mol. Biol. 12, 794–800 (2005). 22. Schmidt, M.J., West, S. & Norbury, C.J. The human cytoplasmic RNA terminal U-transferase ZCCHC11 targets histone mRNAs for degradation. RNA 17, 39-44 (2011).
- 23. Sobti, M., Cubeddu, L., Haynes, P.A. & Mabbutt, B.C. Engineered rings of mixed yeast Lsm proteins show differential interactions with translation factors and U-rich RNA. Biochemistry 49, 2335-2345 (2010).
- 24. Bonner, W.M., Mannironi, C., Orr, A., Pilch, D.R. & Hatch, C.L. Histone H2A.X gene transcription is regulated differently than transcription of other replication-linked histone genes. Mol. Cell. Biol. 13, 984-992 (1993).
- 25. Mannironi, C., Bonner, W.M. & Hatch, C.L. H2A.X. a histone isoprotein with a conserved C-terminal sequence, is encoded by a novel mRNA with both DNA replication type and polyA 3' processing signals. Nucleic Acids Res. 17, 9113-9126 (1989).
- 26. Herrero, A.B. & Moreno, S. Lsm1 promotes genomic stability by controlling histone mRNA decay. EMBO J. 30, 2008-2018 (2011).
- 27. Glasmacher, E. et al. Roquin binds inducible costimulator mRNA and effectors of mRNA decay to induce microRNA-independent post-transcriptional repression. Nat. Immunol. 11, 725-733 (2010).
- 28. Tharun, S. et al. Yeast Sm-like proteins function in mRNA decapping and decay. Nature 404, 515–518 (2000). 29. Song, M.G. & Kiledjian, M. 3' Terminal oligo U-tract-mediated stimulation of
- decapping. RNA 13, 2356-2365 (2007).
- 30. Coller, J. & Parker, R. General translational repression by activators of mRNA decapping. Cell 122, 875-886 (2005).
- 31. Hirai, H., Lee, D.I., Natori, S. & Sekimizu, K. Uridylation of U6 RNA in a nuclear extract in Ehrlich ascites tumor cells. J. Biochem. 104, 991-994 (1988).
- 32. Heo, I. et al. Lin28 mediates the terminal uridylation of let-7 precursor MicroRNA. Mol. Cell 32, 276-284 (2008).
- 33. Jones, M.R. et al. Zcchc11-dependent uridylation of microRNA directs cytokine expression. Nat. Cell Biol. 11, 1157-1163 (2009).
- 34. Heo, I. et al. TUT4 in concert with Lin28 suppresses microRNA biogenesis through pre-microRNA uridylation. Cell 138, 696-708 (2009).



ONLINE METHODS

Mice and cell lines. Mice were housed in specific pathogen-free barrier facilities and used in accordance with protocols approved by the animal-care and state and federal guidelines of the Helmholtz Zentrum München. Sex-, age- and strainmatched wild-type control mice were used in all experiments. T cell–specific $\it Eri1$ -deficient mice ($\it Eri1^{fl/fl}$; $\it CD4Cre$) were on a pure C57BL/6 background. MEF cells were isolated by sacrificing pregnant females 13.5 d $\it post$ coitum and separating the embryos. Fibroblasts of the appropriate genotype were taken into culture and immortalized by ecotropic retroviral infection with SV40 large T antigen, using hygromycin selection at 100 µg/ml for two weeks. MEF and T cells were treated with 5 mM HU, as previously described²0.

RNA isolation, cDNA synthesis and quantitative PCR. RNA was isolated by using Trizol and reverse transcribed with QuantiTect Reverse Transcription Kit (Qiagen), which also removes traces of contaminating genomic DNA. The Roche assay design center (https://www.roche-applied-science.com/sis/rtpcr/upl/ezhome.html) was used to design qPCR assays that were in silico–tested to avoid off-target amplification and that consisted of two primers and a UPL probe (Roche). Supplementary Table 2 lists all primer and probe combinations that were used. Real-time PCR was performed as described for UPL assays (Roche) on a Light Cycler 480II and with Light Cycler 480 software release 1.5.0 SP1, which was used to calculate efficiency-corrected relative expression. For the experiments shown in Figure 1a,d,e and Figure 4a, the $\Delta\Delta C_p$ method was chosen for analysis. If not stated otherwise, Hprt (hypoxanthine guanine phosphoribosyltransferase, NM_013556) and Pbgd (porphobilinogen deaminase, also called hydroxymethylbilane synthase (Hmbs), NM_013551) were used as a reference for relative quantification throughout (Supplementary Table 2).

Oligouridylation qPCR assay. Reverse transcription was performed with 3–5 μ g total RNA at an optimized temperature of 14.4 °C (Supplementary Fig. 3a) for 2 h, using three gene-specific primers—GSP 1h2ak R (5 pmol/ μ l), GSP Hprt1 R (2 pmol/ μ l) and ((A)₁₄-GFP-RT (5 pmol/ μ l) (Supplementary Table 2)—and applying the Superscript III First Strand Synthesis Kit (Invitrogen). Real-time PCR was carried out as advised for UPL assays (Roche) using the primer pairs (U)_n-1h2ak for/rev, Hist1h2ak for/rev and Hprt for/rev (Supplementary Table 2), for which the amplification efficiency was determined as 2.00, 1.93 and 1.95, respectively (Supplementary Fig. 3b). All results were efficiency corrected as described for qPCR (above).

Circularization RT-PCR and cloning. cRT-PCR was performed as depicted in **Figure 2e** and as described²⁰. Circularized *Hist2h4* mRNA was reverse transcribed by using the primer cRT 2H4 RT and PCR amplified (cRT 2H4 PCR for/rev, **Supplementary Table 2**).

Virus production and infection. Retroviral supernatants were produced by calcium phosphate transfection of HEK293T cells with amphotropic packaging and retroviral expression vectors. Supernatants were collected 48 h after transfection, filtered through 0.45-µm filters, supplemented with 5 µg ml $^{-1}$ polybrene and used for infection. Puromycin selection started 48 h after infection, at a concentration of 2 µg ml $^{-1}$, and ended when 100% of uninfected control cells were dead.

T-cell culture and stimulation. Cultures of helper T cells were prepared and analyzed as described 35 . Briefly, CD4+ T cells were purified from spleen and superficial cervical, facial, axillary, brachial and inguinal lymph nodes by magnetic-bead selection (Dynal). Purified T cells were activated with hamster anti-mouse CD3 (0.1 µg/ml; 145-2C11) and anti-mouse CD28 (1 µg/ml; 37N) antibodies cross-linked on goat anti-hamster IgG–coated plates (0.3 mg/ml in PBS at 4 $^{\circ}$ C overnight; MP Biomedicals) for 44 h (Fig. 1b,c) or as described (Fig. 4a). Samples were collected by removing the supernatant and lysing cells in Trizol (Sigma). For the elutriation experiment, cells were activated as described above, and the cultures were supplemented to induce $\rm T_{H}2$ differentiation 27 . After being stimulated for 48 h, cell populations were expanded in recombinant human IL-2 (10 U/ml; World Health Organization, National Institute for Biological Standards and Control). All monoclonal antibodies were purified from supernatants of hybridomas on protein A– or protein G–Sepharose columns and were dialyzed against PBS.

Cell-cycle analysis. $T_{\rm H}^2$ CD4 T cells were stimulated for 40 h. Both $T_{\rm H}^2$ and MEF cells were labeled for 40 min by using BrdU. Further sample preparation was according to the APC BrdU Flow Kit manual (BD Pharmingen).

Co-immunoprecipitation of Lsm1- and Eri1-associated proteins and histone mRNA. Co-immunoprecipitation was performed as previously described³⁶. For each sample, two 15-cm dishes of MEF cells (~80-90% confluent) were washed twice with PBS. Cells were centrifuged (300g, 5 min, 4 °C), and the pellet was lysed in 600–800 μl lysis buffer (20 mM Tris, pH 7.5, 150 mM NaCl, 0.25% (vol/vol) Nonidet-P40, 1.5 mM $MgCl_2$, protease-inhibitor mix without EDTA (Roche) and 1 mM dithiothreitol). Lysates were passaged through a 26-gauge needle, shock frozen, thawed and cleared by centrifugation (4 °C, 10 min, 10,000g). For co-immunoprecipitation of histone mRNA, polyclonal anti-GFP (A11122; Invitrogen) antibody-coupled magnetic beads (Invitrogen) were incubated for 4 h at 4 °C with lysates in the presence of 20 U RNasin (Promega). For co-immunoprecipitation of Eri1-associated proteins, monoclonal anti-Eri1 (5G8) antibody-coupled magnetic beads (Invitrogen) were used and incubated for 4 h at 4 °C with lysates supplemented with or without RNase (Roche). Beads were washed twice (RNA) or three times (protein) with lysis buffer and for RNA co-immunoprecipitation an additional two times with high-salt lysis buffer (300 mM NaCl, 0.5% (vol/vol) Nonidet-P40 and 2.5 mM MgCl₂). For co-immunoprecipitation of Lsm1-associated proteins and histone mRNAs, lysates of untreated or hydroxyurea-treated wildtype and Eri1-deficient MEF cells were incubated with monoclonal anti-Lsm1 (5F3) antibody-coupled magnetic beads (Life Technologies) for 4 h at 4 °C. Beads were washed five times with either lysis buffer (protein) or high-salt lysis buffer (RNA), respectively. To isolate RNA, the pellet (including magnetic beads) was resuspended in 600 µl lysis-and-binding buffer of the MirVana kit (Ambion), and RNA purification was performed according to the manufacturer's manual. Reverse transcription of the RNA for qPCR or for the oligouridylation qPCR assay was performed as described above.

RNA immunoprecipitation for semiquantitative PCR. The procedure was carried out exactly as previously described⁶. The primers 2H4F1 (TTG CGT GAC AAC ATC CAG GG) and 2H4B2 (TTG GCG TGC TCG GTG TAG G) were used to amplify the histone gene *Hist2h4*.

Centrifugal elutriation and flow cytometry. Centrifugal elutriation (Beckman J6-MC centrifuge) was used to separate the different cell-cycle phases of 5×10^8 exponentially growing T_H2-differentiated CD4 T cells as previously described³⁷. Cells were washed with PBS and resuspended in 30 ml RPMI supplemented with 1% FCS, 2 mM EDTA and 0.25 U/ml DNase I (Roche). Cells were injected in a JE-5.0 rotor with a large separation chamber at 1,400 r.p.m. and a flow rate of 29 ml/min, controlled with a Cole-Palmer Masterflex pump. The rotor speed was kept constant, and 400-ml fractions were collected at increasing flow rates (32 (G1-G0), 35 (G1-S), 38 (S), 41 (S-G2) and 44 ml (G2)/minute). Individual fractions were counted and split three ways for flow cytometry (1 \times 10 6 cells), immunoblotting (0.3 to 3.3 \times 10 7 cells) and RNA isolation $(0.4 \text{ to } 2.3 \times 10^7 \text{ cells})$. For flow cytometry, cells were washed once with PBS, resuspended in 1 ml 80% ethanol, 20% PBS and incubated for 1 h on ice. Fixed cells were washed twice with PBS, and 900 µl PBS supplemented with 200 U RNase were added. After 15 min incubation on ice, 100 µl of the propidium iodide stain was added (5 µg/ml PI, 50 mM EDTA in PBS), and samples were kept on ice until the DNA content was determined by using a Becton Dickinson FACS Calibur.

In vitro mRNA transcription and electroporation of MEF cells. In vitro transcription and polyadenylation were performed according to the manufacturer's instructions (Ambion). Single transfections contained 10 μg of the indicated RNA. For double transfections, $10\,\mu g$ of Ch-poly(A) and $10\,\mu g$ of G-2ak-(U)_0_14 were mixed for electroporation (Bio-Rad, Gene Pulser Xcell, exponential protocol, 250 V, 500 μF , 4 mm cuvette) of 4×10^6 MEF cells that were washed in Opti-MEM (Gibco) twice. Fluorescent protein was analyzed by flow cytometry after 24 h, and RNA samples were obtained by lysing cells 4 h, 6 h and 24 h after transfection, using Trizol. Prior to lysis, cells were incubated for 1 h in 2 ml warm cell-culture medium, including $10\,\mu g/ml$ DNase-free RNase (Roche) to degrade RNA outside of the cells. qPCR-based assays to detect Cherry and GFP-fusion transcripts used primers and probes listed in Supplementary Table 2.



npg © 2013

RNA-linker ligation. Total RNA (50 µg) from Eri1-deficient cells was separated on a denaturing agarose gel. RNA of $\sim\!200-800$ nt was purified from a gel slice by using the Gelase high-activity protocol (Epicentre) and performing a subsequent ammonium acetate/ethanol precipitation, according to the instructions of the manufacturer. A universal miRNA cloning linker (New England BioLabs) was ligated to RNA 3' ends by using T4 RNA ligase 1 (ref. 38). cDNA was produced at 48 °C by using Superscript III (Life Technologies) and a reverse primer with the complementary linker sequence, extended by an anchoring 3' adenine (ATT GAT GGT GCC TAC AGA). Standard PCR amplification was performed with a forward primer that annealed in the 3' UTR of Hist1h2ak (TAG AAA GCA ACC

CTT TCC) and the reverse primer above. The PCR products were directly used for TA cloning and sequencing.

- 35. Ansel, K.M. et al. Deletion of a conserved II4 silencer impairs T helper type 1-mediated immunity. Nat. Immunol. 5, 1251–1259 (2004).
- Weinmann, L. et al. Importin 8 is a gene silencing factor that targets argonaute proteins to distinct mRNAs. Cell 136, 496–507 (2009).
- 37. Ritzi, M. *et al.* Complex protein-DNA dynamics at the latent origin of DNA replication of Epstein-Barr virus. *J. Cell Sci.* **116**, 3971–3984 (2003).
- Lau, N.C., Lim, L.P., Weinstein, E.G. & Bartel, D.P. An abundant class of tiny RNAs with probable regulatory roles in *Caenorhabditis elegans*. Science 294, 858–862 (2001).